

Characterization of CRYO ASIC for charge readout in the nEXO experiment

Z. Li¹ M. Yu² E. Angelico³ A. Atencio⁴ A. Gupta² P. Knauss⁵ A. Pena-Perez²
 B. G. Lenardo² P. Acharya⁶ A. Amy^{7,8} A. Anker² I. J. Arnquist⁹ J. Bane⁸ V. Belov¹¹
 T. Bhatta¹³ A. Bolotnikov¹⁴ J. Breslin¹⁵ P. A. Breur² J. P. Brodsky¹² E. Brown¹⁵
 T. Brunner^{17,16} B. Burnell¹⁴ E. Caden^{18,19,17} G. F. Cao^{20,a} L. Q. Cao²¹ D. Cesmecioglu⁸
 D. Chernyak⁶ M. Chiu¹⁴ R. Collister²² M. Marquis¹⁶ T. Daniels²³ L. Darroch²⁴ R. DeVoe³
 M. L. di Vacri⁹ X. Defay² Y. Y. Ding²⁰ D. Doering² M. J. Dolinski⁴ A. Dragone² B. Eckert⁴
 A. Emara²⁵ N. Fatemighomi¹⁸ W. Fairbank²⁷ B. T. Foust⁹ D. Gallacher¹⁷ N. Gallice¹⁴
 A. Gaur²² W. Gillis^{8,b} F. Girard¹⁷ A. Gorham⁹ K. Gracequist²² G. Gratta³ C. A. Hardy^{3,c}
 J. Hasi² S. Hedges¹² M. Heffner¹² E. Hein²⁹ H. Hernandez Herrera² J. D. Holt^{16,17}
 A. Iverson²⁷ X. S. Jiang²⁰ A. Karelina¹¹ D. Kebelbeck³⁰ C. Kenney² I. Kotov¹⁴
 A. Kuchenkov¹¹ K. S. Kumar⁸ S. Lavoie¹⁷ A. Larson³¹ M. B. Latif^{4,d} K. G. Leach³⁰
 D. S. Leonard³³ G. Lessard¹⁰ K. K. H. Leung³⁴ G. Li²⁰ X. Li¹⁶ C. Licciardi²⁵ R. Lindsay³⁵
 R. MacLellan¹³ S. Majidi¹⁷ C. Malbrunot^{16,17} B. Markovic² J. Masbou⁷
 M. Medina-Peregrina⁵ S. Mngonyama³⁵ B. Mong² D. C. Moore²⁴ K. Ni⁵ I. Nitu¹⁷ A. Nolan⁸
 S. C. Nowicki¹⁷ J. C. Nzobadila Ondze³⁵ A. Odian² J. L. Orrell⁹ G. S. Ortega⁹ L. Pagani⁹
 H. Peltz Smalley⁸ A. Piepke⁶ A. Pocar⁸ S. Prentice¹⁰ V. Radeka¹⁴ E. Raguzin¹⁴ R. Rai¹⁷
 H. Rasiwala¹⁷ D. Ray^{17,16} B. Reese² S. Rescia¹⁴ F. Retiere¹⁶ G. Richardson²⁴ V. Riot¹²
 R. Ross¹⁷ L. Rota² P. C. Rowson² R. Saldanha⁹ S. Sangiorgio¹² S. Sekula^{38,18} T. Shetty²⁵
 L. Si³ F. Spadoni⁹ V. Stekhanov¹¹ X. L. Sun²⁰ S. Thibado⁸ T. Totev¹⁷ S. Triambak³⁵
 R. H. M. Tsang^{6,e} O. A. Tyuka³⁵ T. Vallivilayil John^{19,22} E. van Bruggen⁸ M. Vidal³ S. Vie²²
 M. Walent¹⁹ H. Wang²⁰ Q. D. Wang²¹ M. Watts²⁴ W. Wei²⁰ M. Wehrfritz²⁹ L. J. Wen²⁰
 S. Wilde²⁴ X. M. Wu²¹ H. Xu⁵ H. B. Yang²¹ L. Yang⁵ O. Zeldovich¹¹ J. Zhao²⁰

¹Department of Physics and Astronomy, University of Hawaii at Manoa, Honolulu, HI 96822, USA

²SLAC National Accelerator Laboratory, Menlo Park, CA 94025, USA

³Physics Department, Stanford University, Stanford, CA 94305, USA

⁴Department of Physics, Drexel University, Philadelphia, PA 19104, USA

⁵Physics Department, University of California San Diego, La Jolla, CA 92093, USA

⁶Department of Physics and Astronomy, University of Alabama, Tuscaloosa, AL 35405, USA

⁷SUBATECH, Nantes Université, IMT Atlantique, CNRS/IN2P3, Nantes 44307, France

^aAlso at: University of Chinese Academy of Sciences, Beijing, China

^bNow at: Bates College, Lewiston, ME 04240, USA

^cNow at Yale University, New Haven, CT 06511, USA

^dAlso at: Center for Energy Research and Development, Obafemi Awolowo University, Ile-Ife, 220005 Nigeria

^eNow at: Canon Medical Research USA, Inc.

⁸*Amherst Center for Fundamental Interactions and Physics Department, University of Massachusetts, Amherst, MA 01003, USA*

⁹*Pacific Northwest National Laboratory, Richland, WA 99352, USA*

¹⁰*Université de Sherbrooke, Sherbrooke, QC J1K 2R1, Canada*

¹¹*National Research Center “Kurchatov Institute”, Moscow, 123182, Russia*

¹²*Lawrence Livermore National Laboratory, Livermore, CA 94550, USA*

¹³*Department of Physics and Astronomy, University of Kentucky, Lexington, KY 40506, USA*

¹⁴*Brookhaven National Laboratory, Upton, NY 11973, USA*

¹⁵*Department of Physics, Applied Physics, and Astronomy, Rensselaer Polytechnic Institute, Troy, NY 12180, USA*

¹⁶*TRIUMF, Vancouver, BC V6T 2A3, Canada*

¹⁷*Physics Department, McGill University, Montréal, QC H3A 2T8, Canada*

¹⁸*SNOLAB, Lively, ON P3Y 1N2, Canada*

¹⁹*School of Natural Sciences, Laurentian University, Sudbury, ON P3E 2C6, Canada*

²⁰*Institute of High Energy Physics, Chinese Academy of Sciences, Beijing, 100049, China*

²¹*Institute of Microelectronics, Chinese Academy of Sciences, Beijing, 100029, China*

²²*Department of Physics, Carleton University, Ottawa, ON K1S 5B6, Canada*

²³*Department of Physics and Physical Oceanography, University of North Carolina Wilmington, Wilmington, NC 28403, USA*

²⁴*Wright Laboratory, Department of Physics, Yale University, New Haven, CT 06511, USA*

²⁵*Department of Physics, University of Windsor, Windsor, ON N9B 3P4, Canada*

²⁶*Oak Ridge National Laboratory, Oak Ridge, TN 37831, USA*

²⁷*Physics Department, Colorado State University, Fort Collins, CO 80523, USA*

²⁸*Physikdepartment and Excellence Cluster Universe, Technische Universität München, Garching 80805, Germany*

²⁹*Skyline College, San Bruno, CA 94066, USA*

³⁰*Department of Physics, Colorado School of Mines, Golden, CO 80401, USA*

³¹*Department of Physics, University of South Dakota, Vermillion, SD 57069, USA*

³²*Department of Physics and Astronomy, McMaster University, Hamilton, ON L8S 4M1, Canada*

³³*IBS Center for Underground Physics, Daejeon, 34126, South Korea*

³⁴*Department of Physics and Astronomy, Montclair State University, Montclair, NJ 07043, USA*

³⁵*Department of Physics and Astronomy, University of the Western Cape, P/B X17 Bellville 7535, South Africa*

³⁶*School of Physics and Astronomy, Shanghai Jiao Tong University, Shanghai 200240, China*

³⁷*Erlangen Centre for Astroparticle Physics (ECAP), Friedrich-Alexander University Erlangen-Nürnberg, Erlangen 91058, Germany*

³⁸*Department of Physics, Queen’s University, Kingston, ON K7L 3N6, Canada*

³⁹*LHEP, Albert Einstein Center, University of Bern, 3012 Bern, Switzerland*

⁴⁰*Institut für Kernphysik, Westfälische Wilhelms-Universität Münster, Münster 48149, Germany*

ABSTRACT: nEXO is a proposed next-generation experiment searching for the neutrinoless double beta decay of ^{136}Xe using a tonne-scale liquid xenon (LXe) time projection chamber (TPC). To image the ionization signals from events in the liquid xenon, the detector will employ metallized fused-silica charge collection tiles instrumented with cryogenic application-specific integrated circuits (ASICs), referred to as CRYO ASIC, which are designed to operate directly in LXe to minimize input capacitance and pick-up noise. Here we present the performance of the CRYO ASIC mounted on an auxiliary printed circuit board and evaluated both in a cryogenic environmental chamber and in a dedicated LXe test stand. We demonstrate that the ASICs achieve the desired performance at liquid xenon temperatures, showing a gain stability better than 0.2% over 24-hour operation and reliable in-situ calibration using an on-chip pulser. In the LXe test stand, we show that boiling caused by the chip heat dissipation can be mitigated by operating the system above ~ 0.1 MPa. The in-LXe noise measured agrees with simulation, which indicates it the $150 e^-$ design requirement can be satisfied. These results establish CRYO ASIC as a viable low-noise in-LXe charge readout solution for nEXO.

KEYWORDS: Cryogenic detectors, Noble liquid detectors, Neutrino detectors, Front-end electronics for detector readout

Contents

| | | |
|----------|---|-----------|
| 1 | Introduction | 1 |
| 2 | Experimental Apparatus | 3 |
| 2.1 | CRYO ASIC Cold Board | 3 |
| 2.2 | CRYO ASIC FEMB board | 4 |
| 2.3 | Liquid nitrogen-cooled cryogenic chamber | 5 |
| 2.4 | Liquid xenon test stand | 5 |
| 3 | Results | 7 |
| 3.1 | CRYO ASIC functionality tests in cryogenic chamber | 7 |
| 3.2 | CRYO ASIC gain calibration and stability test | 8 |
| 3.3 | Study of boiling conditions during liquid xenon operation | 9 |
| 3.4 | Noise measurement with CRYO ASIC in liquid xenon | 10 |
| 4 | Summary and outlook | 11 |
| 5 | Acknowledgments | 12 |

1 Introduction

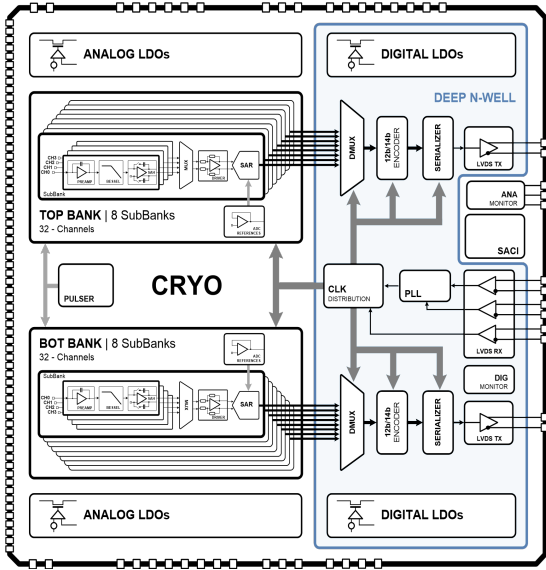
nEXO is a proposed experiment to search for neutrinoless double beta ($0\nu\beta\beta$) decay of ^{136}Xe using five tonnes of liquid xenon (LXe) and a time projection chamber (TPC), designed to achieve a half-life sensitivity beyond $T_{1/2} \sim 10^{28}$ years [1]. $0\nu\beta\beta$ decay is a hypothetical process in which a nucleus with mass A and charge Z undergoes the decay $(A, Z) \rightarrow (A, Z+2) + 2e^-$ without emission of neutrinos [2]. Its discovery would constitute direct evidence of lepton-number violation and establish that neutrinos are Majorana particles [3]. In nEXO, particle interactions in the LXe produce prompt scintillation light, detected by silicon photomultipliers (SiPMs) surrounding the barrel of the TPC volume, and ionization charges, which will drift to a segmented charge-sensing anode under an cylindrical electric field. The event energy will be reconstructed from a linear combination of the scintillation and ionization signals, while the three-dimensional position and event topology will be determined from the anode charge collection patterns (x, y) and the timing difference between the two signals (z). The anode of the nEXO TPC will be composed of an array of $\sim 10 \times 10$ cm fused silica charge-collection tiles patterned with gold electrodes, forming orthogonal 6 mm pitch strips in the x and y directions [4]. In total, 3,840 independent readout channels will need to be processed.

The charge readout system design is driven by three primary requirements: 1) achieving an overall energy resolution better than 1% at the $\beta\beta$ Q-value of 2.458 MeV, 2) enabling effective background discrimination, and 3) maintaining extremely low radioactivity. To achieve sub-1%

energy resolution requires limiting electronic noise to below $150\text{ }e^-$ equivalent noise charge. For preserving waveform shape information which is crucial for topological background rejection, a 2 MHz digitization rate and anti-aliasing filter characteristics are selected, as well as a 12-bit dynamic range up to 50 fC based on simulations of signal and background events. Prototype ASICs fabricated in the TSMC 130 nm CMOS process contain sub-ppt intrinsic contamination of both ^{238}U and ^{232}Th chains [5], and operating the front-end electronics directly in LXe minimizes cabling and associated radioactive and electronegative impurities. Thus, nEXO is developing cryogenic application-specific integrated circuits (ASICs), referred to as CRYO ASIC, for in-LXe charge readout.

CRYO ASIC is a System-on-Chip (SoC) 64-channel waveform digitizer and serializer, designed for TPC experiments operating at cryogenic temperatures [6, 7]. The functional block diagram of the ASIC is illustrated in Fig. 1 alongside the key specifications for the nEXO experiment. Fabricated in 130 nm CMOS process, The ASIC integrates both analog and digital functions with a minimal number of I/Os. The analog section is organized into two identical banks, top and bottom, each containing 32 channels and delivering a single data output stream. Within each bank, the channels are grouped into eight sub-banks of four channels each. Every channel includes a dedicated analog front-end circuit, with analog multiplexing used to share a single 12-bit ADC among four channels with 8MSPS sampling rate. The outputs from the eight ADCs (covering 32 channels) are then processed by a digital back-end module, which performs digital multiplexing, DC-balancing encoding, and serialization in DDR (Double Data Rate) format. To comply with the stringent low-radioactivity requirements, the design employs on-chip supply regulation by distributing low-dropout (LDO) voltage regulators across the chip, ensuring stable power delivery to the core sections while minimizing the need for external components. The size of the CRYO ASIC is $6774\text{ }\mu\text{m} \times 8948\text{ }\mu\text{m}$ (including the pad frame) and it dissipates about 1.27 W (20 mW/ch) at 165 K from a 2.5 V power supply. A future 32-channel version of the chip is expected to reduce the power consumption to 15 mW/ch. The ASIC has been designed using techniques outlined in Ref. [8] to extend lifetime at cryogenic temperatures, such as operating internal blocks at reduced voltage (2 V and 1 V for analog and digital blocks, respectively) and using devices larger than the minimal length in critical areas. Beyond these reliability considerations, the ASIC architecture has also been developed with testability in mind. To support this, dedicated inputs and outputs have been included to enable independent evaluation and calibration of key building blocks across temperature conditions. An analog monitor output allows for measuring internal voltage signals, such as the front-end output waveform of any selected channel. It also provides access to key analog signals, including the internal supply regulation voltages and the reference signals driving the ADCs. An internal pulser system is integrated to facilitate assessment of the front-end channel performance. Furthermore, digital monitor outputs, similar to the analog monitor, allow for inspection of critical clock and control signals during operation. To ensure stable operation across a wide temperature range, the ASIC integrates a custom serial communication interface developed at SLAC National Accelerator Laboratory(SACI [9]), which enables the user to directly program the core sections in real time through internal registers.

In this paper, we present the cryogenic testing of the CRYO ASIC using two different test systems. In section 2 we describe the two different ASIC data acquisition (DAQ) systems, as well as the gas nitrogen environmental chamber and the liquid xenon test stand used in this work. Section 3



| Parameter | Specification |
|----------------------|---|
| Process | 130 nm CMOS |
| Supply voltage | 2.5 V (2 V, 1 V internal) |
| Input capacitance | $\sim 20 \text{ pF} - 30 \text{ pF}$ |
| Anti-aliasing filter | 5th order Bessel architecture |
| Peaking times | 0.6 μs , 1.2 μs , 2.4 μs , 3.6 μs |
| Gain settings | 9.6 mV/fC, 14.3 mV/fC, 28.6 mV/fC, 57.2 mV/fC |
| Max. input charge | 150 fC, 100 fC, 50 fC, 25 fC |
| Noise | $< 150 e^-$ @ 28.6 mV/fC and 1.2 μs |
| ADC | 12-bit 2 MSPS / CH |
| INL and DNL | $\pm 1 \text{ LSB}$ |
| Power consumption | < 20 mW/CH |
| Temperature | LXe $\sim 160 \text{ K}$ (-113 $^{\circ}\text{C}$) |

Figure 1. Functional block diagram of the CRYO ASIC and the design specifications of the nEXO-specific implementation.

describes measurements results demonstrating the gain stability and noise performance of CRYO ASIC.

2 Experimental Apparatus

The nEXO experiment's strict radiopurity and mechanical requirements will necessitate extreme control of materials used for external components and cabling. For testing purposes, however, we use commercial printed circuit boards with off-the-shelf discrete components, and use loading capacitors to characterize the front-end performance under realistic conditions. These systems are described in detail here.

2.1 CRYO ASIC Cold Board

The CRYO ASIC Cold Board is a multi-layer printed circuit board (PCB) designed to incorporate power regulators, input circuitry, and the CRYO ASIC. Fig. 2 shows the Cold Board with one CRYO ASIC directly mounted and wire-bonded to the board. The use of bare dies is adopted since conventional ASIC packaging exceeds the radiopurity requirement of nEXO. The Cold Board supports two power schemes. In one scheme, an internal low-dropout regulator (LDO) provides the main 2.5 V supply to the CRYO ASIC. In the second scheme, the internal LDOs of the ASIC are disabled, and external LDOs supply 2 V to the analog circuitry and 1 V to the digital circuitry, powering the internal sections of the ASIC directly. For ASIC characterization, the board is configured to use the first power scheme by default. To simulate the channel capacitance in the nEXO detector, the 64 input channels of the CRYO ASIC are loaded with 22 pF ($\pm 1\%$) or 33 pF ($\pm 1\%$) C0G ceramic capacitors, whose values change by less than 0.3% when cooled down to LXe temperature ($\sim 160 \text{ K}$).

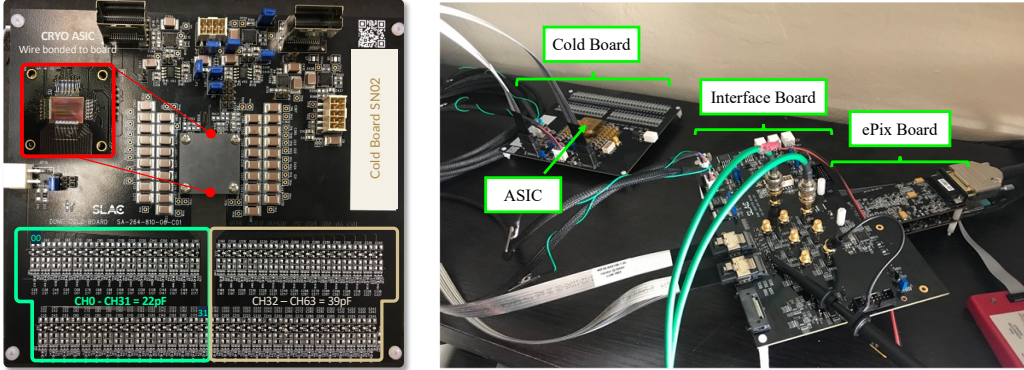


Figure 2. Photo of the CRYO ASIC Cold Board system. Left: The CRYO ASIC mounted on a custom PCB (Cold Board) and a zoom view of the ASIC wire bonded to the board below a protective cover. The 64 input channels are loaded with 22 pF or 33 pF capacitors. Right: the cold board communicates with the ePix board and the adapter board for data acquisition.

The programming and testing are conducted using a Linux desktop computer connected by fiber to a custom ePix Field Programmable Gate Arrays (FPGA) board [10]. The ePix board interfaces with an adapter board to supply power to the Cold Board and enable communication between the Linux desktop computer and the Cold Board. Data and control signals are transmitted using two high speed twin axial cables [11]. The CRYO ASIC monitoring is essential to optimize the internal registers and ensure operation and performance at both room and LXe temperatures. Before regular testing and operation, the ASICs go through an initial period of calibration in which the internal registers are adjusted so that the voltage levels of the internal LDOs, verified through analog and digital monitor outputs, closely match the expected design values. Once calibrated, the registers remain fixed and loaded into the ASIC during the initialization process for the given temperature conditions. The register control and programming of the ASIC are managed through the SACI protocol [9]. The Linux desktop is configured with the open-source SLAC SURF [12] and ROGUE [13] environments to support firmware development and data acquisition.

2.2 CRYO ASIC FEMB board

A second CRYO ASIC test board is the Front-End Mother Board (FEMB) that allows the characterization of two ASICs simultaneously, as shown in Fig. 3. Similar to the Cold Board, the FEMB power distribution is regulated by LDOs strategically placed across the board, following the same power scheme configuration as the Cold Board. During the characterization, the ASICs operate with their internal supply regulation by default and the FEMB board supplies the main 2.5 V. Instead of placing input capacitors directly between the ground and individual channel inputs like on the Cold Board, FEMB has the ASIC inputs routed to connectors on the backside, which are directly coupled to each individual channel, allowing convenient connection to different input loads.

The data acquisition (DAQ) setup for the FEMB board follows a configuration similar to that of the Cold Board. A commercial KCU 105 FPGA board [14] replaces the custom ePix board, reducing cost while improving compatibility across different test platforms. To drive the FEMB, the adapter board is reconfigured to enable communication and control through the commercial FPGA.

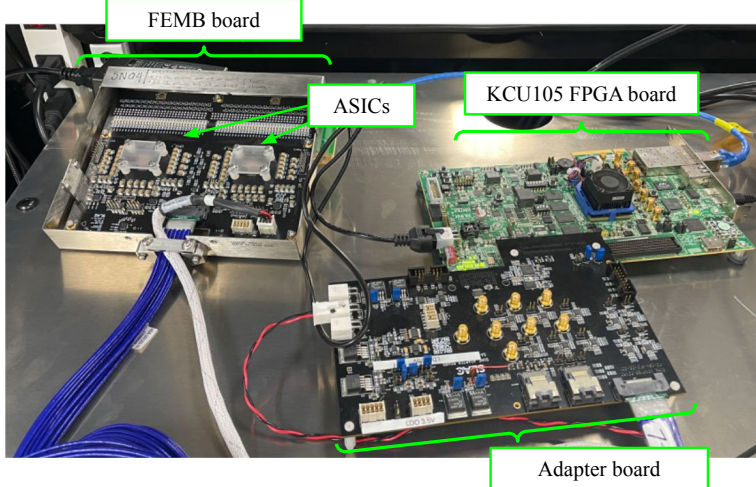


Figure 3. The CRYO ASIC FEMB Board is enclosed in an RF shielded box, with the two CRYO ASICs protected beneath acrylic covers. It interfaces with the adapter board and is controlled via the commercial FPGA board.

The FPGA connects to the adapter board via a high-density open-pin-field array connector [15], while a single custom SAMTEC cable serves as the interface between the FEMB and the adapter board, transmitting both control and data signals. Power cabling and the software environment remain consistent with the Cold Board system.

2.3 Liquid nitrogen-cooled cryogenic chamber

A liquid-nitrogen cooled cryogenic chamber [16] shown in Fig. 4 is used to test ASIC boards in a nitrogen gas environment at the LXe temperature of 160 K. The chamber uses liquid nitrogen evaporation cooling and trim heating for temperature control, with a fan recirculating the coolant in a vertical flow at $4.25 \text{ m}^3/\text{min}$ 150 CFM to maintain temperature uniformity. It features adjustable temperature ramp rates, enabling quick and precise control of the temperature within the chamber. The chamber's metal case provides shielding from environmental radio-frequency (RF) noise. When testing the Cold Board, an additional metal box surrounding the Cold Board is used to provide further RF shielding. The FEMB board is already protected with an RF shield box. A temperature sensor can be installed inside the metal boxes during tests to directly monitor the temperature of the ASIC Boards.

2.4 Liquid xenon test stand

To replicate the nEXO environment, a dedicated test stand is constructed for in-liquid-xenon testing at the University of California San Diego. The test stand consists of a xenon gas handling system, an inner LXe chamber, and an outer HFE-7000 cryostat, similar to those described in Ref. [17]. Fig. 5 (left) shows a photo of the LXe chamber installed in the outer cryostat, and Fig. 5 (right) shows the schematic drawing of the LXe chamber. The inner chamber is built from a 25.4 cm ConFlat spool-piece and two flanges. The body of the chamber is made of 304 stainless steel, with an inner diameter of 20 cm and a height of 12 cm. The top flange includes a gas feedthrough for xenon filling.

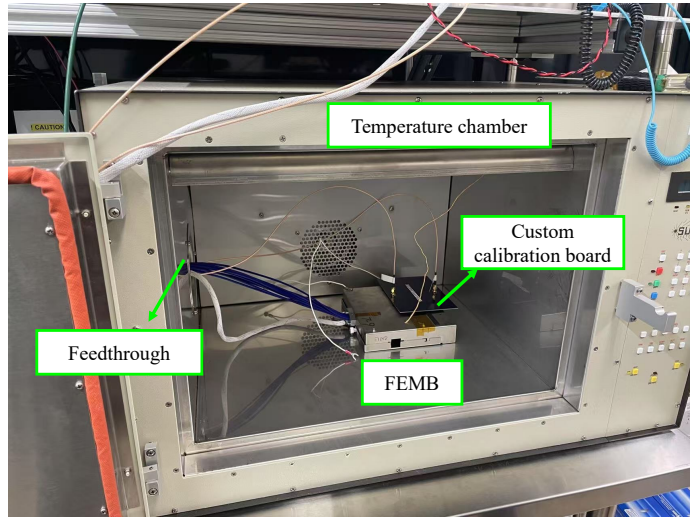


Figure 4. A photo of the liquid nitrogen-cooled cryogenic test chamber. The FEMB board is placed in the chamber connected to the DAQ system at room temperature. An external calibration board (purple), plugged into the back of the FEMB board for gain calibration studies, can also be seen in the photo.

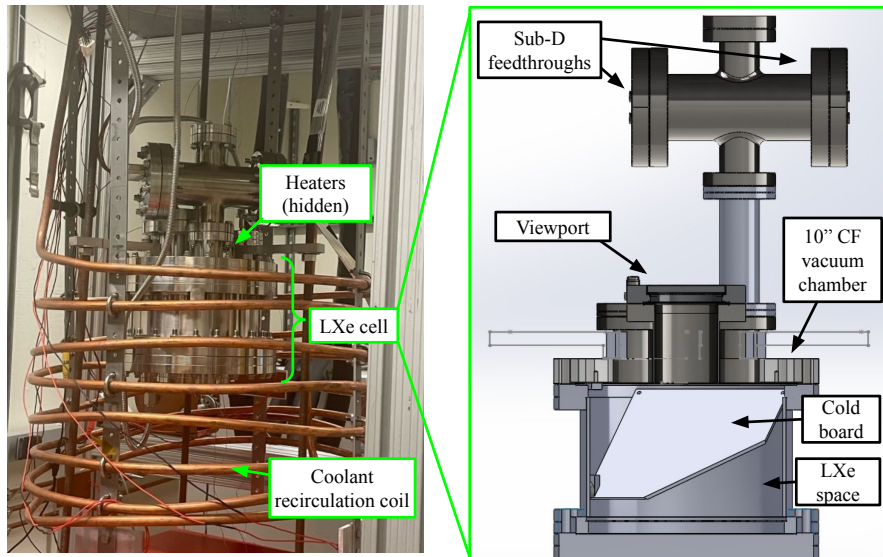


Figure 5. Liquid xenon test stand for CRYO ASIC testing. Left: Photo of the inner LXe chamber installed in the outer cryostat. Right: schematic drawing of the inner LXe chamber and placement of the cold board inside the chamber.

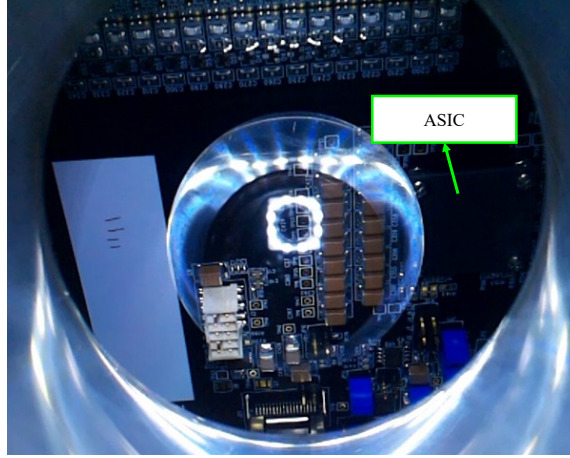


Figure 6. An image of the Cold Board immersed in LXe taken by the monitoring camera through the viewport. The halo observed in the center of the photo is light from LEDs surrounding the camera being reflected from the LXe surface.

and recovery, a ConFlat 4-way reducing cross, and a ConFlat quartz viewport. The 4-way reducing cross has two 50-pin (25-pin \times 2) D-type feedthroughs, allowing connection of four custom cables terminated with a D-type connector that links the Cold Board to the adapter board. An Arducam Motorized Focus Pi OV5647 Camera [18] is mounted above the viewport to visually monitor the CRYO ASIC and LXe conditions. The camera is controlled and read by a Raspberry Pi outside the outer cryostat. The bottom flange has a second gas feedthrough for xenon filling and recovery. The inner chamber is filled with \sim 7 kg of LXe to fully submerge the CRYO ASIC on the Cold Board. Fig. 6 shows a photo of the Cold Board immersed in LXe, taken by the monitoring camera through the viewport.

The test stand is typically operated at \sim 168 K and at varied pressures below 0.15 MPa. Mimicking the cryogenic scheme used in EXO-200 and proposed for nEXO [19], the LXe chamber is submerged in HFE-7000 cooling fluid to maintain good temperature uniformity. The HFE-7000 is contained in a cryostat and cooled via a large copper coil immersed in the HFE-7000, which recirculates coolant from a Telemark Model 1800 cryochiller. Four thermocouples, three attached at different points on the inner chamber and one placed at the bottom of the HFE-7000 in the outer chamber, measure the system temperature. A PID loop, managed by a LabVIEW application, adjusts the coolant flow based on measurements from the thermocouple mounted in the middle of the LXe chamber to regulate the system temperature.

3 Results

As suggested by simulations, a gain of 28.6 mV/fC is one of the preferred configurations for nEXO. All subsequent measurements are performed under this setting.

3.1 CRYO ASIC functionality tests in cryogenic chamber

Both the Cold and the FEMB boards are tested in the cryogenic chamber. Tests using the Cold Board mainly consisted of register level optimization for different temperatures from room temperature

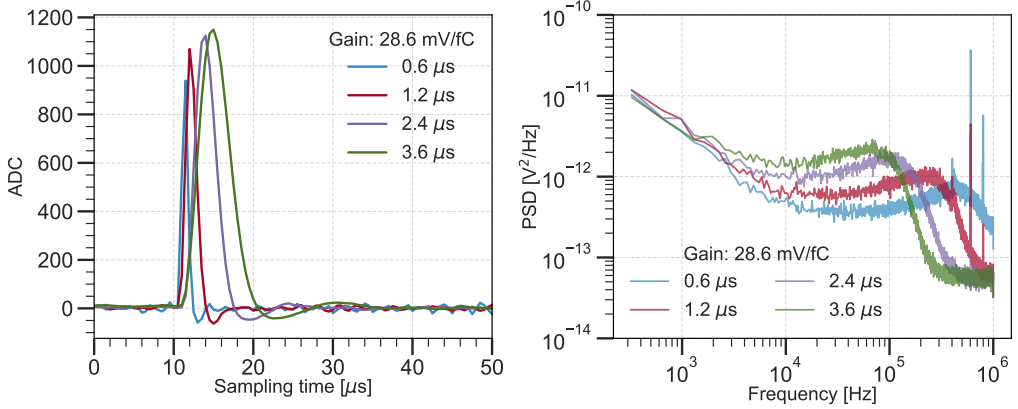


Figure 7. Sample waveforms from FEMB board with internal pulses (left) and corresponding noise power spectral density (right) of four peaking time settings with 28.6 mV/fC gain.

down to 160 K. The same settings can be used for the LXe chamber tests at those temperatures. The FEMB board is used for more comprehensive testing, aimed at studying the long-term stability of the ASIC at LXe temperature. A photo of the FEMB Board test in the cryogenic chamber can be seen in Fig. 4.

The functionality of both the Cold and FEMB boards is verified in this system. The internal charge pulser system on the ASIC is used to verify different settings for each channel, including combinations of four gain settings and four peaking times. Fig. 7 (left) shows sample waveforms of four peaking time configurations with the internal pulser at a gain of 28.6 mV/fC taken with the FEMB Board. Fig. 7 (right) shows the corresponding noise power spectral density (PSD). As expected, the bandwidth of the output signals decreases as the peaking time of the anti-aliasing filter increases.

3.2 CRYO ASIC gain calibration and stability test

Achieving nEXO’s target energy resolution requires calibrating the gain of each channel to within 0.2%, with recalibrations performed periodically throughout the planned 10 year operation. An internal pulser system is implemented in the CRYO ASIC to monitor all front-end channels over time, as shown in the block diagram in Fig. 1. Each channel has a separate pulser composed of a programmable DAC, a test capacitor, and a switch. The amplitude and on/off of the internal pulser can be controlled through the internal register using SACL. To verify the stability of the internal pulser, an external calibration system is implemented to inject charge directly into the front-end channel inputs. A custom calibration board, connected to the SAMTEC connector of the FEMB board and shown in Fig. 4, is designed to simultaneously inject charge into 64 channels. For each channel, a 22 pF capacitor is connected between the channel input and the ground to simulate the detector capacitance. A 1 pF capacitor is connected in series between the channel input and an external pulser to convert voltage inputs into charge signals. All capacitors are COG to minimize temperature variation, and traces for all channels on the calibration board are designed with nearly matched lengths to ensure that contributions from parasitic capacitances, which are estimated around 2-3 pF, are uniform.

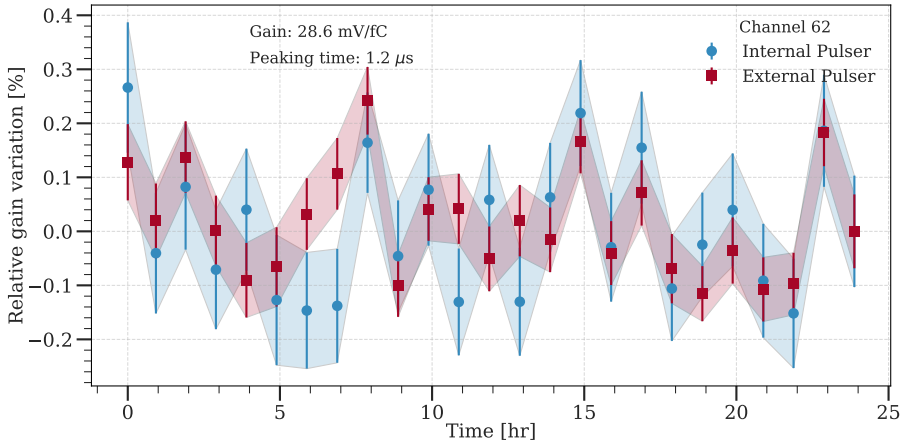


Figure 8. Relative variation of the input gain over time, arbitrarily normalized to the last data point. Channel 62 is shown as an example, where the gain is set as 28.6 mV/fC and the peaking time is 1.2 μ s. The calibration results with the internal pulser and the external pulser are plotted in blue and red respectively. The RMS variation variation of the internal and external pulser are 0.12% and 0.10%, respectively, meeting the <0.2% variation requirement for nEXO. Furthermore, we observe correlation between the two signals, indicating that the internal pulser can provide reliable in-situ calibration.

The gain stability test is carried out for 24 hours in the cryogenic N₂ chamber at 160 K. The gains are measured with both the internal and the external pulser calibration systems once every hour. Approximately 40 fC of charge is injected from either the internal or external pulsers. The external pulser used a square waveform with a 40 mV_{pp} amplitude and a 3 kHz frequency. Approximately 3000 waveforms are recorded for each pulser calibration run and analyzed offline. The peaks in the waveforms are fitted with a Gaussian function to extract the pulse amplitudes. For each channel, the relative change of the average waveform amplitudes over time is referred to as the gain variation. Data are taken with the front end channels configured with 28.6 mV/fC gain and 1.2 μ s peaking time. The measurements show that the RMS gain variation on all channels is less than 0.2% during the 24-hour testing period. Fig. 8 shows the gain variation of a representative channel, and the remaining channels show similar behavior. The calibration data from the two pulser systems track each other well, indicating that the stability of the internal pulser is sufficient for gain stability monitoring at the 0.2% level.

3.3 Study of boiling conditions during liquid xenon operation

In the nEXO TPC, a key concern is the heat dissipation from these electronics, which can create local boiling conditions and potentially generate microphonic noise in the electronics or cabling, or lead to electrical breakdown in high electric fields. A dedicated measurement of the onset of nucleate boiling in LXe is performed [20] to understand boiling conditions. To evaluate the LXe boiling induced by the CRYO ASIC's power dissipation and explore the mitigation strategies, a Cold Board is tested in the LXe test stand with the CRYO ASIC immersed in LXe with its protective cover removed. The LXe is visually monitored by the camera through the viewport on the top flange of the LXe chamber and quantitatively measured by a temperature sensor and a pressure gauge. The



Figure 9. Left: a screenshot of the camera monitoring the LXe condition, where ripples from boiling are clearly visible. Right: a screenshot of the camera showing the LXe condition with no visible boiling from the ASIC.

noise is measured under approximately the same temperature and pressure immediately after the camera is turned off, eliminating pickup noise from the camera in the ASIC front-end.

Significant boiling is observed after the CRYO ASIC is powered on, following stabilization of the LXe's pressure at 0.095 MPa, and temperature at 170.45 K, as shown in the left figure of Fig. 9. A larger noise is measured on the CRYO ASIC correlated to the boiling, which is shown in Fig. 10.

To increase the gas pressure in the chamber, two polyimide flexible adhesive heaters on the top flange of the LXe chamber are turned on to apply heat to the liquid. Because the HFE-7000 is filled below the top flange, the temperature of the HFE-7000 and the inner volume of the LXe chamber had an insignificant increase due to the heaters. The increased temperature of the top flange resulted in a higher pressure of 0.104 MPa inside the chamber, which effectively suppressed the LXe boiling. The mitigation of LXe boiling is evident from both the camera monitoring and the CRYO ASIC noise measurement. A photo of the LXe from the monitoring camera is shown in the right panel of Fig. 9. As nEXO is expected to operate at approximately 165 K and pressures around 0.15 MPa [21], we conclude that CRYO ASIC will not induce boiling in the experiment.

3.4 Noise measurement with CRYO ASIC in liquid xenon

The noise performance of CRYO ASIC is studied in the LXe chamber by increasing the system pressure to eliminate the boiling issue. Multiple measurements are carried out when it is found through the monitor camera that the chip is fully submerged in the liquid. During the measurements, the conditions of the system are carefully monitored to ensure that no xenon boiling occurs.

The noise PSD spectra from the xenon temperature tests are shown in Fig. 10, with a gain of 28.6 mV/fC and a peaking time of 0.6 μ s to capture the full frequency-domain response. Higher noise power is observed for larger loading capacitance, as expected. The simulated PSD curve for a 40 pF capacitance load is shown as the green line in the right panel, illustrating good agreement between in-LXe data and design simulations.

The standard deviation (STD) of the baseline fluctuations from the ASICs, in units of ADC counts, can be converted to an equivalent noise charge (ENC), as shown in Fig. 11. As expected, the noise level of channels 0–31 (top bank), loaded with 22 pF, is lower than that of channels 32–63

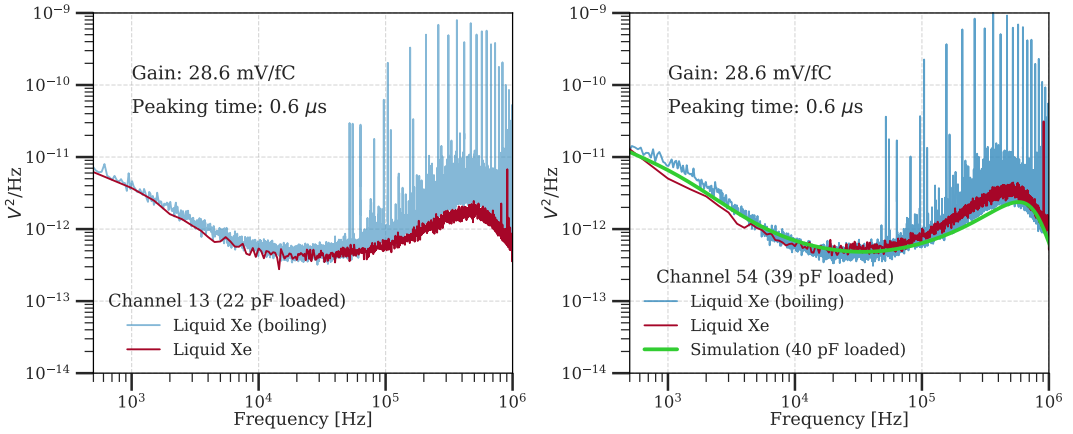


Figure 10. Noise PSD of two individual channels on the top bank and the bottom bank, respectively, at 165 K, where the front-end channels are set with 28.6 mV/fC gain and 0.6 μ s peaking time. Left plot: channel 13 at the top bank (22 pF capacitor loaded). Right plot: channel 54 at the bottom bank (39 pF capacitor loaded). The simulated spectrum is shown as the green line, which agrees well with the measurements. The influence of the liquid boiling issue can be observed on the blue curves.

(bottom bank), which are loaded with 39 pF. One dead channel (channel 33) has been excluded from the plot. As nEXO is most likely to read out the charge signal with either 0.6 μ s or 1.2 μ s peaking time in order to preserve the waveform integrity, we present noise measurements corresponding to these two configurations. Data taken with a 1.2 μ s peaking time exhibits lower ENC than that with a 0.6 μ s peaking time, due to stronger suppression by the anti-aliasing filter. Channels with the same load and peaking time show a \sim 10% variation in noise, attributed to differences in wirebonding and trace lengths. By incorporating the parasitic trace capacitance on the Cold Board, simulated noise values across the channels in each bank are shown as gray lines. The small negative slope in the simulations is in good agreement with the data. For 22 pF loading capacitance, the predicted ENC values are \sim 185 e^- for 0.6 μ s peaking time and \sim 156 e^- for 1.2 μ s peaking time, and the corresponding values are \sim 263 e^- and \sim 210 e^- for 39 pF loading capacitance from the recent simulation [22]. As shown in Fig. 11, our liquid xenon testing yields noise ENC that matches the simulation results well, which indicates that the nEXO charge module can meet the experimental requirements.

4 Summary and outlook

The CRYO ASIC performance has been characterized using both the Cold Board and the FEMB board in a cryogenic chamber and a liquid xenon test stand. The ASIC demonstrates stable operation at room temperature and at cryogenic temperature relevant to nEXO. In the cryogenic chamber at 160 K, the channel gain remains stable over 24-hour operation, and the on-chip charge injection pulser provides a stable method for in-situ calibration. During operation in liquid xenon, heat dissipation from the ASIC was initially observed to induce localized xenon boiling, which results in elevated noise. This effect is mitigated by pressurizing the chamber while minimizing the temperature increase, restoring the CRYO ASIC to optimal noise performance. With operation pressures around

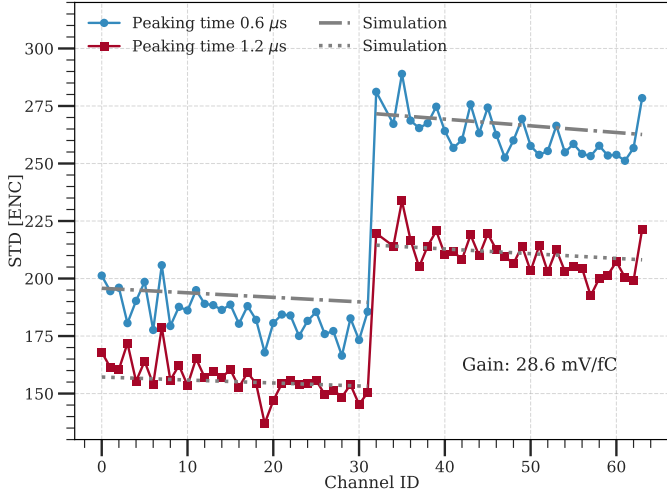


Figure 11. Noise ENC of all 64 channels on the cold board for four tests at 168 K with 28.6 mV/fC gain, both 0.6 μ s (red markers) and 1.2 μ s (blue markers) peaking times. Channels 0-31 are loaded with $C_{\text{load}} = 22$ pF and channels 32-63 are loaded with $C_{\text{load}} = 39$ pF. The gray horizontal lines represent the simulation results. The negative slope on the ENC with respect to the channel ID comes from trace capacitance of the cold board.

0.15 MPa, we conclude that no boiling will be induced in nEXO. Under these conditions, the ASIC achieves an average noise performance of 156 e^- ENC at a gain of 28.6 mV/fC, 1.2 μ s peaking time, and 22 pF input capacitance. The measured noise in LXe agrees with design simulations, which indicates that the nEXO charge module can meet the experimental requirements.

Future work will involve testing the ASICs coupled to sensor tiles for ionization readout, as well as tests involving the radiopure cables [23] and mechanical assemblies that will be required for deployment in the actual nEXO experiment. However, the tests described in this paper demonstrate that the CRYO ASIC can achieve low-noise and stable performance when operated directly in LXe, validating its suitability for in-LXe charge readout in nEXO.

5 Acknowledgments

The authors thank Mark Convery (SLAC) for his significant contributions to the development of the FEMB system, and Bob Conley (SLAC) for his dedicated support in the setup and configuration of the cryogenic testing. G. R. and A. A. were supported by the U.S. Department of Energy Science Graduate Student Research through contract number DE-SC0014664. M.Y. and B.L. are supported by the Department of Energy, Laboratory Directed Research and Development program at SLAC National Accelerator Laboratory, under contract DE-AC02-76SF00515. This work was also supported in part by Laboratory Directed Research and Development (LDRD) programs at Brookhaven National Laboratory (BNL), Lawrence Livermore National Laboratory (LLNL), Pacific Northwest National Laboratory (PNNL), and SLAC National Accelerator Laboratory. The authors gratefully acknowledge support for nEXO from the Office of Nuclear Physics within DOE’s Office of Science under grants/contracts DE-FG02-01ER41166, DE-SC002305, DE-FG02-93ER40789, DE-SC0021388, DE-SC0012704, DE-AC52-07NA27344, DE-SC0017970,

DE-AC05-76RL01830, DE-SC0012654, DE-SC0021383, DE-SC0014517, DE-SC0024666, DE-SC0020509, DE-SC0024677 and support by the US National Science Foundation grants NSF PHY-2111213 and NSF PHY-2011948; from NSERC SAPPJ-2022-00021, CFI 39881, FRQNT 2019-NC-255821, and the CFREF Arthur B. McDonald Canadian Astroparticle Physics Research Institute in Canada; from IBS-R016-D1 in South Korea; and from CAS in China.

References

- [1] nEXO collaboration, [nEXO: neutrinoless double beta decay search beyond \$10^{28}\$ year half-life sensitivity](#), [J. Phys. G 49 \(2022\) 015104](#) [[2106.16243](#)].
- [2] W.H. Furry, [On transition probabilities in double beta-disintegration](#), [Phys. Rev. 56 \(1939\) 1184](#).
- [3] J. Schechter and J.W.F. Valle, [Neutrinoless Double beta Decay in SU\(2\) x U\(1\) Theories](#), [Phys. Rev. D 25 \(1982\) 2951](#).
- [4] nEXO collaboration, [Characterization of an Ionization Readout Tile for nEXO](#), [JINST 13 \(2018\) P01006](#) [[1710.05109](#)].
- [5] nEXO Collaboration, [In preparation](#), 2025.
- [6] A. Pena-Perez, A. Gupta, B. Markovic, L. Rota, D. Doering, M. Convery and A. Dragone, [CRYO: A System-on-Chip for Charge Readout in the nEXO Experiment](#), in [2022 IEEE Nuclear Science Symposium \(NSS\), Medical Imaging Conference \(MIC\) and Room Temperature Semiconductor Detector \(RTSD\) Conference](#), 11, 2022, [DOI](#).
- [7] D. Doering, A. Pena-Perez, E. Angelico, A. Gupta, L. Ruckman, L. Rota, B. Markovic, J. Segal, C. Kenney and A. Dragone, [CRYO ASIC for Noble Liquid Time Projection Chamber Test Setup and Characterization](#), in [2022 IEEE Nuclear Science Symposium \(NSS\), Medical Imaging Conference \(MIC\) and Room Temperature Semiconductor Detector \(RTSD\) Conference](#), 11, 2022, [DOI](#).
- [8] LBNE collaboration, [Cryogenic Lifetime Studies of 130 nm and 65 nm nMOS Transistors for High-Energy Physics Experiments](#), [IEEE Trans. Nucl. Sci. 62 \(2015\) 1255](#).
- [9] B. Reese, A. Dragone, A. Gupta, B. Markovic and A. Pena-Perez, [Saci: A serial interface for asic configuration](#), in [2023 IEEE Nuclear Science Symposium, Medical Imaging Conference and International Symposium on Room-Temperature Semiconductor Detectors \(NSS MIC RTSD\)](#), pp. 1–1, 2023, [DOI](#).
- [10] K. Nishimura, G. Blaj, P. Caragiulo, G. Carini, A. Dragone, G. Haller, P. Hart, J. Hasi, R. Herbst, S. Herrmann et al., [Design and performance of the epix camera system](#), in [AIP Conference Proceedings](#), vol. 1741, AIP Publishing, 2016.
- [11] 3M Twin Axial Cable Assembly for Internal miniSAS Applications (8F36 Series) .
- [12] SURF: SLAC Ultimate RTL Framework, .
- [13] Rogue: SLAC Python Based Hardware Abstraction & Data Acquisition System, .
- [14] AMD Kintex UltraScale FPGA KCU105 Evaluation Board, .

- [15] Samtec High Density Terminal Array Assembly,
<https://www.digikey.com/en/products/detail/samtec-inc/ASP-134604-01/9762396>.
- [16] Sun Electronic Systems Temperature Test Chamber, Model EC02,
<https://www.sunelectronics.com/Temperature-Test-Chamber-EC02-Model.html>.
- [17] E. Angelico, J. Dalmasson, R. DeVoe, G. Gratta, C.A. Hardy, B. Lenardo, L. Si, M. Vidal and S. Wu,
A flexible test facility for liquid xenon detector development, [JINST **20** \(2025\) P11005](https://doi.org/10.1088/1748-0221/20/11/P11005) [[2508.05853](#)].
- [18] Arducam Auto Focus Pi Camera, OV5647 5MP 1080P, <https://www.arducam.com/product/raspberry-pi-camera-5mp-autofocus-motorized-focus-camera-b0176/>.
- [19] EXO-200 collaboration, The EXO-200 detector, part II: auxiliary systems, [JINST **17** \(2022\) P02015](https://doi.org/10.1088/1748-0221/17/02/P02015) [[2107.06007](#)].
- [20] P.A. Breur, G.S. Ortega, P.C. Rowson, R. Saldanha, B. Mong, M. Oriunno and C. Mo,
Measurement of the onset of nucleate boiling in liquid xenon, [JINST **16** \(2021\) T02004](https://doi.org/10.1088/1748-0221/16/02/T02004) [[2007.11124](#)].
- [21] nEXO collaboration, nEXO Pre-Conceptual Design Report, [1805.11142](#).
- [22] A.P. Perez, Cryo asic: A system-on-chip (soc) for charge readout in the nexo experiment, in
Coordinating Panel for Advanced Detectors (CPAD) Workshop, 2023.
- [23] I.J. Arnquist, M.L. di Vacri, N. Rocco, R. Saldanha, T. Schlieder, R. Patel, J. Patil, M. Perez and
H. Uka, Ultra-low radioactivity flexible printed cables, [EPJ Tech. Instrum. **10** \(2023\) 17](https://doi.org/10.1051/epj/2023170) [[2303.10862](#)].